Designing porous-crystalline structure of β-Ga2O3: a potential approach to tune its opto-electronic properties

Journal:	*Physical Chemistry Chemical Physics*
Manuscript ID	CP-ART-12-2017-008565.R2
Article Type:	Paper
Date Submitted by the Author:	02-Mar-2018
Complete List of Authors:	Banerjee, Swastika; E O Lawrence Berkeley National Laboratory, Materials Sciences Division Jiang, Xiang-Wei; Institute of Semiconductors, Chinese Academy of Sciences, State Key Laboratory of Superlattices and Microstructures Wang, Lin-Wang; Lawrence Berkeley National Laboratory,

Journal Name

ARTICLE TYPE

Cite this: DOI: 10.1039/xxxxxxxxxx

Designing porous-crystalline structure of β-Ga_2O_3: a potential approach to tune its opto-electronic properties†

Swastika Banerjee,*[a] Xiangwei Jiang,*[b] and Lin-Wang Wang*[c]

Received Date
Accepted Date

DOI: 10.1039/xxxxxxxxxx

www.rsc.org/journalname

β-Ga_2O_3 has drawn recent attention as a state-of-art electronic material due to its stability, optical transparency and appealing performance in power devices. However, it has also found a wider range of opto-electronic applications including the photocatalysis especially in its porous forms. For such applications, a lower band gap must be obtained and the electron-hole spatial separation would be beneficial. Like many other metal oxides (e.g., Al_2O_3), Ga_2O_3 can also form various types of porous structures. In the present study, we investigate how its optical and electronic properties can be changed in a particular porous structure with stoichiometrically balanced extended vacancy-channels. We apply a set of first principles computation methods to investigate the formation, structural, dynamic, and opto-electronic properties. We find that such extended vacancy channel is mechanically stable and has relatively low formation energy. We also find that it results in a spatial separation of the electron and hole, forming a long-lived charge transfer state that has the desirable characteristics for photocatalyst. In addition, the electronic band gap reduces to VIS-region unlike the transparency in pure β-Ga_2O_3 crystal. Thus, our systematic study promises the application of such porous structure of β-Ga_2O_3 as a versatile electronic material.

1 Introduction

Gallium oxide (Ga_2O_3) has proven itself as a state-of-art wide band gap (~5.0 eV) semiconductor due to its excellent performance in power device applications.[1,2] Optical transparency in Ga_2O_3 arises from the large electronegativity difference between Ga and O atoms, as well as the strong Ga-O bonding. However, there are possible alternate usage for this stable and green material. For example, Ga_2O_3 serves the purpose of a transition metal free photocatalyst for CO_2 reduction due to its high reduction potential for CO_2.[3,4] Ga_2O_3 has also been attempted to be used as a catalyst for conversion of CO_2 to CH_4[5,6] as well as water-splitting[7]. Indeed, instead of the transition metals with a open shell d-state, metal oxide photocatalysts with d^{10} configurations (In^{3+},Ga^{3+}, Ge^{4+}, Sn^{4+}, Sb^{5+}) are of great interest. This is because the hybridization between the s and p orbital of metals in the conduction band could enhance the mobility of photogenerated electrons, thus, producing high photocatalytic activity.[8–10] Compared to transition metal oxides, they also have a lesser tendency to form small polarons.[11,12] However, insufficient availability of the reaction sites in bulk gallium oxide remain as an issue to achieve high efficiency for catalytic reactions. The attempts to solve this problem include the reconstruction of the material into porous form, or as a nanostructure.[13–15] Many oxides, e.g. the well known Al_2O_3, can be synthesized into a variety of porous structures.[16,17] The same is expected for Ga_2O_3. Although the mechanism of the higher activity of porous structure can be qualitatively understood as the enhancement of the surface-active sites, there are other changes in its electronic and optical properties which are also important. It is thus extremely interesting to study the differences of their electronic and optical properties to their crystal counter parts, and to find the potential applications of this material beyond power-devices. In addition, versatile applications of oxides in optoelectronics and photocatalysis also necessitate a tunable band gap and the visible light sensitivity.[18–20] The pure crystalline Ga_2O_3 has a too large optical

[a] Materials Sciences Division, Lawrence Berkeley National Laboratory, 1 Cyclotron Road, Berkeley, CA 94720, USA, E-mail: swastikabanerjee@lbl.gov
[b] Institute of Semiconductors, Chinese Academy of Sciences, Beijing 100083, China, E-mail: xwjiang@semi.ac.cn
[c] Materials Sciences Division, Lawrence Berkeley National Laboratory, 1 Cyclotron Road, Berkeley, CA 94720, USA, E-mail: lwwang@lbl.gov

† Electronic Supplementary Information (ESI) available: [Validation of present model, Computational details, Results & discussion on larger pore model, The Brillouin zone of the monoclinic $\beta - Ga_2O_3$, PBE band structure plots, Nature of VBM-1, VBM, and CBM at the gap state (Γ-point)

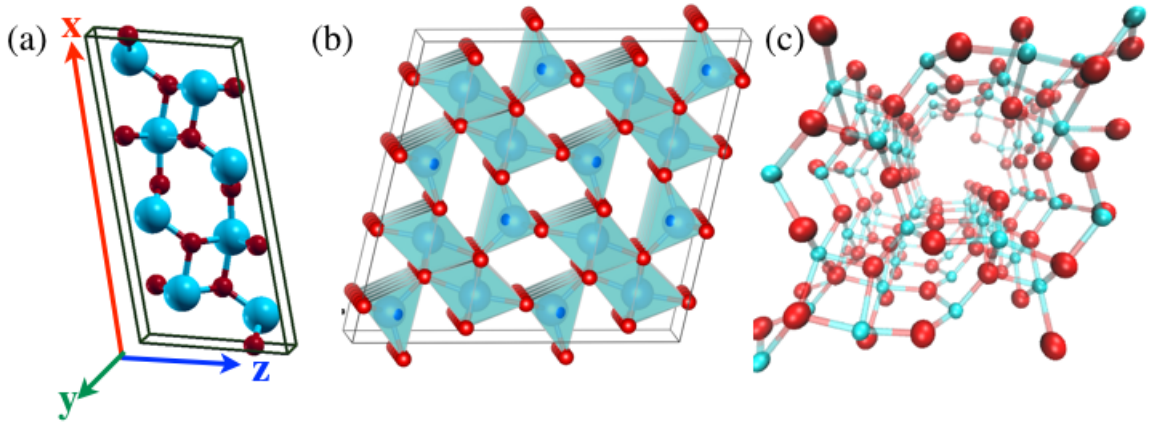

Fig. 1 (a) The primitive unit cell of monoclinic β-Ga_2O_3. Ga and O atoms are represented by cyan and red spheres, respectively. β is defined as the angle between x and z axis. (b) 1x4x2 supercell is considered to model the one dimensional vacancy channel (as shown in c) in β-Ga_2O_3.

band gap for any VIS-light applications. It is thus important to see whether some type of porous Ga_2O_3 also reduces its optical band gap.

According to the literatures, the base-centred monoclinic β-Ga_2O_3 with $C2/m$ symmetry (see Figure 1) is the most stable phase at ambient condition among all the polymorphs, namely, α, β, γ, δ and ε.[21–23] During synthesis, different kinds of vacancy-defects arise inevitably.[6,24] Interestingly, in the case of β-Ga_2O_3, vacancies nucleate at a very fast rate which also results in the possibility of forming porous channel (as shown in cartoon Figure 1c).[25–27] This motivates us to use the vacancy-channel as a model to study the porous channel and porous structure of Ga_2O_3, and how such structure affects the opto-electronic properties of the system. In the present study, we have designed a β-Ga_2O_3 based system which combines both the crystallinity as well as porous nature in the structural framework. In this sense, our current approach differs from the designing of a material which relies on either pure crystals or completely disordered amorphous. On the other hand, the porous structures, as found in Al_2O_3, can often have many different patterns depending on the synthesis conditions. Our vacancy-channel corresponds to a particular simple pattern of the porous structures. Nevertheless, the point vacancy-defects often result in the charge-excess or charge-deficiency due to non-stoichiometry, and the complete amorphous Ga_2O_3 can also suffer from a serious stability-issue[28]. In contrast, the vacancy-channel can be made stoichiometrically balanced and thus, thermodynamically as well as mechanically stable. So far, we do not know the exact condition to synthesize such vacancy-channel in Ga_2O_3, but that does not prevent us from using it as a model system to study the porous Ga_2O_3, especially as we will show the formation energy of such vacancy channel is rather small. The charge trapping and electron-hole separation in such charge-neutral porous system are also exciting in terms of both the fundamental understanding as well as for practical applications.[29,30] This also represents a new strategy to avoid the use of heavy doping[31] to control the defect-chemistry of semiconductors.

The main objective of this paper is two-folds. One is to shed light on the porous-crystallinity as a new design principle to realise a versatile functional material. Porous Ga_2O_3 can indeed be made, and it can have major applications. One example is reported by Park *et al.*,[6] where the pores are used as CO_2 reduction sites. In practice, the current experimentally achievable pores in Ga_2O_3 is much larger than the one we studied in the present manuscript, but we should never under estimate the ingenuity of our experimental colleagues, especially in the synthesis of nanostructure shapes etc. For example, similar parallel pore channels have been synthesized in Al_2O_3.[32] In comparison with Al_2O_3, pore size of Ga_2O_3 is typically smaller. However, the smallest pore size can be around 4nm.[16,33] Very small channels with the size similar to ours do exist in other materials. For example, less than 1 nm channel exist in carbonaceous material[34] as also evident from the pioneering work, entitled as, "Anomalous Increase in Carbon Capacitance at Pore Sizes Less Than 1 Nanometer". On the other hand, we have witnessed the synthesis of many amazing nano structures with the size scale similar to the one we studied (carbon nano-stripe, nano-flower etc) using novel techniques like molecule assembly etc. Indeed, one can imagine a single molecule activated etching which might lead to a very fine channel. Sometimes what needed is the motivation to synthesise such novel structures. One of the purposes of theoretical study is to calculate the properties of such structures prior to their synthesis, which in turn can motivate the synthesis of such structures. Besides, as we have shown in the calculation, the formation energies of such nano-channels are rather small, much smaller than the point defects. Thus, there is no fundamental reason to say such system cannot be synthesised. We hope our theoretical work can serve as an inspiration. From thermodynamic analysis, we first study which extended channel is most likely to be formed in practice. This also gives us some ideas about how does the most likely porous-channel structure look.

Secondly, we analyse the impact of the porous channel on the optoelectronic properties of β-Ga_2O_3. Here, we propose an way to achieve the VIS-sensitivity in otherwise optically transparent pure β-Ga_2O_3. In particular, we discovered an interesting feature of β-Ga_2O_3 with channel porosity: a long-lived charge transfer

state that has the desirable characteristics for photocatalytic applications. Studying such materials for light-harvesting relies on accurate prediction of band gap. It is computationally challenging to study our porous-crystalline system with large number of atoms, especially, when nonlocal hybrid functionals like HSE06 is used. Herein, we have deployed a new GPU implementation[40] of the hybrid DFT-functional HSE06 for large system calculations. The paper is organized as follows. Section II briefly introduces the theoretical methods and the computational details. Section III presents the calculated results and discusses the findings. Finally, we summarise in Section IV.

2 Computational details

2.1 First principles simulation details

The structural and electronic properties of β-Ga_2O_3 are calculated using density functional theory as implemented in Quantum Espresso (QE) code.[35] For the exchange-correlation potential, we have used the Generalised Gradient Approximation (GGA) as parametrized by Perdew-Burke-Ernzerhof (PBE).[36,37] Band structure details have been obtained with both the PBE functional as well as the Heyd-Scuseria-Ernzerhof (HSE)06 functional[38,39] as implemented in PWmat using GPU.[40] Norm conserved pseudopotentials with energy cutoff of 50 Ry and density cutoff of 200 Ry have been used for all the calculations in PWmat at HSE level. We found that the HSE06 screened Coulomb hybrid functional with a α=0.35 could produce the band gap corroborating with experimental bulk Ga_2O_3 band gap. For all the pwscf calculations at PBE level (in QE), we use the projector-augmented-wave (PAW) pseudopotential[41] with an energy cutoff of 60 Ry for the plane-wave basis sets. Gamma-centred 8 x 4 x 4 Monkhorst-Pack k-point meshes are used for the structural optimisation of 20 atom primary cell. The supercell (1 x 4 x 2) containing 160 atom have been adopted for modelling the vacancy channel present in the β-Ga_2O_3. Further details on the "Validation of present model" has been discussed in the ESI. Gamma-centred 3 x 3 x 3 Monkhorst-Pack k-point meshes are used for structural optimisation of 1 x 4 x 2 supercell. Finer kpoint-mesh (10 x 10 x 10) have been used for computing the band dispersion patterns and density of states. Similar kpoint-meshes have been adopted for PWmat computations unless otherwise stated. It is worth to note that although band gap, E_g, of β-Ga_2O_3 under GGA approximation (2.45 eV) is far below the HSE result (or experimental value), the band dispersion pattern calculated by PBE (see ESI Figure 2) exhibit similar curves to those calculated by HSE06 (see Figure 5). Hence, we extend our study to understand the nature of the electronic states (wavefunctions, density of states and projected density of states) based on the PBE/PAW method, instead of the HSE06 method.

All atomic positions and lattice constants are optimized using the Broyden-Fletcher-Goldfarb-Shanno (BFGS) algorithm, with the total energy and atomic forces minimised. In the presence or absence of the vacancy, atomic positions are fully relaxed with DFT-D2 dispersion correction[42]. The convergence criteria for total energy was chosen to be less than 1 x 10^{-5} eV between two consecutive steps, and the maximum Hellmann-Feynman forces acting on each atom were less than 0.02 eV $Å^{-1}$ upon ionic relaxation. The relaxed atomic structure provide lattice parameters consistent with the experimental measurements.[43]

To calculate the formation energies of the defects and the vacancy-channels, we use an approach based on PBE calculations, which empirically correct the energies of reference elemental-phases (FERE).[44] This method significantly improves the formation energies for compounds and alloys when compared with experiments. With FERE, the predicted formation energy ($\Delta H_f^{FERE}(A_{x_1}B_{x_2}...)$) can be expressed as,

$$\Delta H_f^{FERE}(A_{x_1}B_{x_2}...) = E_{tot}^{GGA}(A_{x_1}B_{x_2}...) - \sum_i x_i \mu_i^{FERE} \quad (1)$$

$$\mu_i^{FERE} = \mu_i + \delta\mu_i^{FERE} \quad (2)$$

In another word, there will be a correction on the direct GGA calculated formation energy $\Delta H_f^{GGA}(A_{x_1}B_{x_2}...)$ by a sum of the FERE elemental phase energy correction, $\delta\mu_i^{FERE}$, weighted by the stoichiometric factors x_i of the respective elements in the compound:

$$\Delta H_f^{FERE}(A_{x_1}B_{x_2}...) = \Delta H_f^{GGA}(A_{x_1}B_{x_2}...) - \sum_i x_i \delta\mu_i^{FERE} \quad (3)$$

The convex hull energy, E_{hull}, for a given A_xB_{1-x} compound on the E(x) curve will determine whether this compound is thermodynamically stable or unstable. If $E_{hull} > 0$ eV/atom, the system is unstable or metastable.

To understand the optical properties, complex dielectric function, $\varepsilon(\omega)$ is calculated,

$$\varepsilon(\omega) = \varepsilon_1(\omega) + i\varepsilon_2(\omega) \quad (4)$$

The dielectric properties are calculated using the first-order time dependent perturbation theory. In this procedure, the dipolar transition matrix elements between the occupied and the unoccupied single electrons are computed using the SIESTA code within the Kohn-Sham (KS) formalism.[45–47] The self-consistent ground state DFT energies and eigenfunctions have been plugged into the dipolar matrix elements. The imaginary part of the dielectric function (ε_2) has been calculated using,

$$\varepsilon_2(\omega) = \frac{4\pi^2 e^2}{m\omega^2} \sum_{i,j} \int < i|M|j >^2 f_i(1-f_i) \times \delta(E_{i,k} - E_{j,k} - \omega) d^3k \quad (5)$$

where, e and m are the charge and mass of free electrons, respectively, and ω is the frequency of incident photon. M is the dipole matrix, where i and j are the initial and final states. f_i is the fermi distribution function for i-th state with wave vector k. The real part (ε_1) is calculated with the help of the Kramers-Kronig (KK) transformation.

$$\varepsilon_1(\omega) = 1 + \frac{2}{\pi} P \int_0^\infty \frac{\omega' \varepsilon_2(\omega') d\omega'}{(\omega'^2 - \omega^2)} \quad (6)$$

where, P denotes the principal value of the integral. Optical properties, such as, the absorption coefficient $\alpha(\omega)$ and the refractive

index $n(\omega)$ have been derived from the dielectric function

$$\alpha(\omega) = \sqrt{2}\omega[\sqrt{\varepsilon_1(\omega)^2 + \varepsilon_2(\omega)^2} - \varepsilon_1(\omega)]^{\frac{1}{2}} \quad (7)$$

$$n(\omega) = \frac{1}{\sqrt{2}}[\sqrt{\varepsilon_1(\omega)^2 + \varepsilon_2(\omega)^2} - \varepsilon_1(\omega)]^{\frac{1}{2}} \quad (8)$$

The optical calculations are done by using a 10 x 10 x 10 optical mesh and 0.2 eV optical broadening. Although the above optical absorption spectrum calculation based on single particle formalism does not include the electron-hole correlation excitonic effects, it should be sufficient to study the change from bulk Ga_2O_3 to the Ga_2O_3 with vacancy-channels. Further detailed comparison between the electronic structure calculations using the Norm-Conserving pseudo potential/atom-centred basis set as implemented in SIESTA and the PAW pseudo potential in Quantum Espresso has been provided in ESI.

3 Results and discussion

3.1 Structure

The structure of bulk β-Ga_2O_3 can be demonstrated with four lattice parameters, i.e, x, y, z and β as described in the the optimized conventional cell in Figure 1(a). Our findings on the structural parameters are in good agreement with previous theoretical[24] and experimental results[48] (see Table 1) which indicate that the optimization method applied in this study is reasonable. The crystalline structure can be visualised in terms of GaO_6 octahedron and GaO_4 tetrahedron chains, which appears anisotropic as viewed from three different crystallographic orientations (see Figures 2a-c). Oxygen ions arrange themselves in a distorted cubic packing and Gallium ions occupy distorted octahedral and tetrahedral sites, as shown in Figure 2b.[49]. There are three inequivalent sites occupied by O, exhibiting two threefold and one fourfold coordination modes. All the Gallium atoms are bonded with four oxygen atoms. The formation of both the Oxygen vacancy (V_O) as well as Gallium vacancy (V_{Ga}) together can lead to 1D vacancy channel (porous-crystalline structure)[6,27] in β-Ga_2O_3 along different directions. We construct the defective structures exhibiting 1D-channels (along x, y and z directions) after forming the 1 x 4 x 2 supercell (see Figure 2d-f) which have been referred to the porous-crystallinity throughout the discussion.

Table 1 Structural parameters of β-Ga_2O_3 and the previous experimental findings.

System	x	y	z	β
Ga_2O_3 (This study)	12.11	3.02	5.73	103.6
Ga_2O_3 (Exp)	12.23	3.04	5.84	103.7

3.2 Stability of porous-crystalline structure:

At first, we would like to study which porous channel is most likely to be formed. We note that the extended vacancy can have different possibilities, i.e. stoichiometric or off-stoichiometric defect concentration of V_O vs. V_{Ga} with respect to the chemical stoichiometry in pure Ga_2O_3. Herein, we investigate the feasibilities of the various vacancy channel structures by computing their formation energies (ΔH_f^{FERE}) while considering: (a) different directions of vacancy channels as well as (b) different ratio of V_O vs. V_{Ga}. Computed results on the energetics explain that stoichiometric defect (see Figure 3) leading to 1D vacancy channel along y-direction, V-2 (C in Figure 3), is the thermodynamically most stable case. Followed by this finding, we have computed and compared the formation energy of stoichiometric defect channels along different crystallographic directions (see Table 2). Nevertheless, there will be always a distribution of all the possibilities depending their relative stability, synthesis condition and reaction kinetics at finite temperature. Evidently, the stability of vacancy channel along y (V-2) lies only 0.10 eV/atom above the Hull (which is the pure β-Ga_2O_3) and is superior to the other two directions (x and z). This means that the stoichiometric V-2 like porous structure is very easy to form and our further discussion will focus on the properties of V-2. To study the kinetic stability, we have carried out *ab-initio* molecular dynamics simulations. From the analysis of radial pair distribution function, g(r), as shown in Figure 4a, there is evidence of well defined peaks without significant broadening. Thus, 1D-vacancy channel in V-2 remains stable without any further defect formation or reconstruction. However, the fluctuation in the pore diameters is found from the trajectory of the channel-surface ions (see Figure 4b,c) due to a floppy mode of vibration. Collective motion of the Ga-/O-ion near the vacancy channel results in the mean value of pore diameter to fluctuate in the range of 4.4-5.8 Å as described in Figure 4c. The oscillation in pore-diameter exhibits a soft channel breathing motion with a period of $\sim$0.3 ps. Such a soft mode is most probably caused by the cutting of the bond in the channel.

Table 2 Formation energy (ΔH_f^{FERE}) and alteration in band gap (ΔE_g) for pure β-Ga_2O_3 and three different 1D vacancy channels along x (V-1), y (V-2) and z (V-3) directions.

System	ΔH_f^{FERE}	ΔE_g
β-Ga_2O_3	-2.29	0.0
V-1	-1.90	-1.24
V-2 (C)	-2.19	-1.65
V-3	-1.91	-1.52

3.3 Electronic Structures

Bulk β-Ga_2O_3 exhibits an wide band-gap of 4.80 eV, as shown in Figure 5a. Both the Valence Band maximum (VBM) and the conduction band minimum (CBM) are situated at the Γ point, meaning that the material belongs to the direct band gap semiconductor which is consistent with the previous experimental results.[50] In line with our findings, several theoretical studies arrived at the similar conclusion that the conduction-band minimum in β-Ga_2O_3 is located at the Γ point and the valence band is almost flat. However there are few disagreements on the position of the valence band maximum in the literature.[51] We note that due to the small dispersion of the valence band, even if the the exact location of VBM is proposed to be at off-Γ point, it does only differ

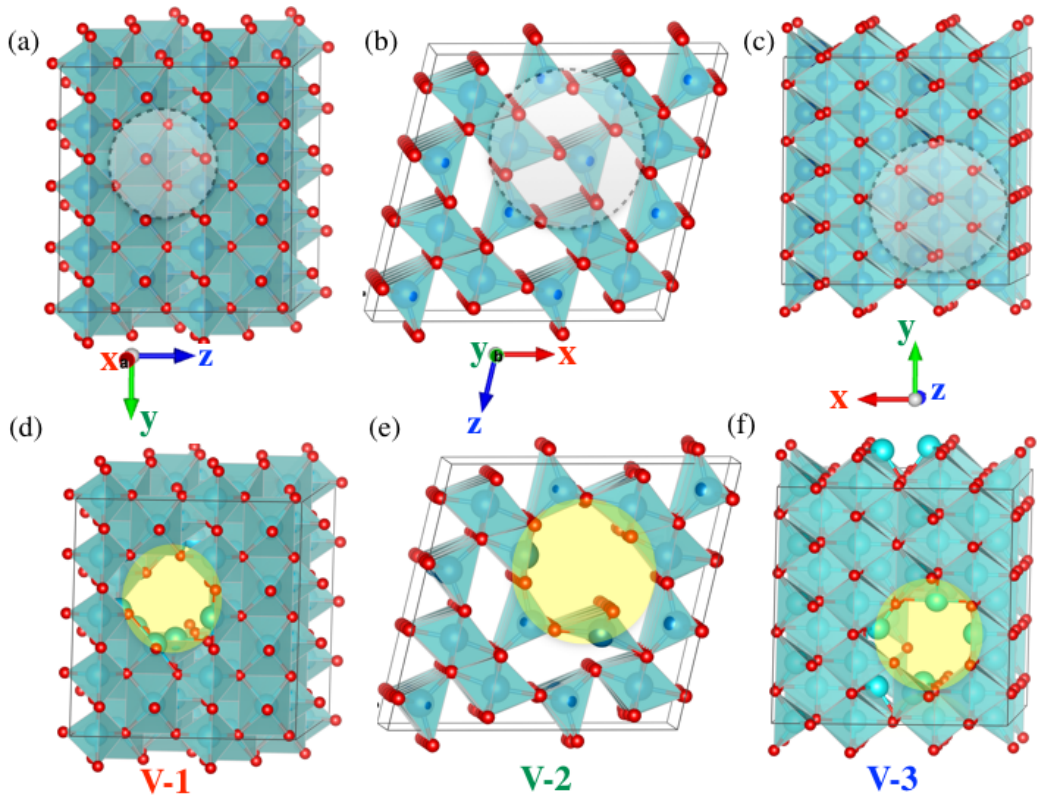

Fig. 2 View along different crystallographic directions of 1x4x2 supercell of monoclinic β-Ga_2O_3: (a) along x, (b) along y, and (c) along z. The atoms which are removed to form the vacancy channels have been indicated using lighter colour. Optimised structures with 1D vacancy channels along different directions: (d) V-1 (along x), (e) V-2 (along y), (f) V-3 (along z) are shown.

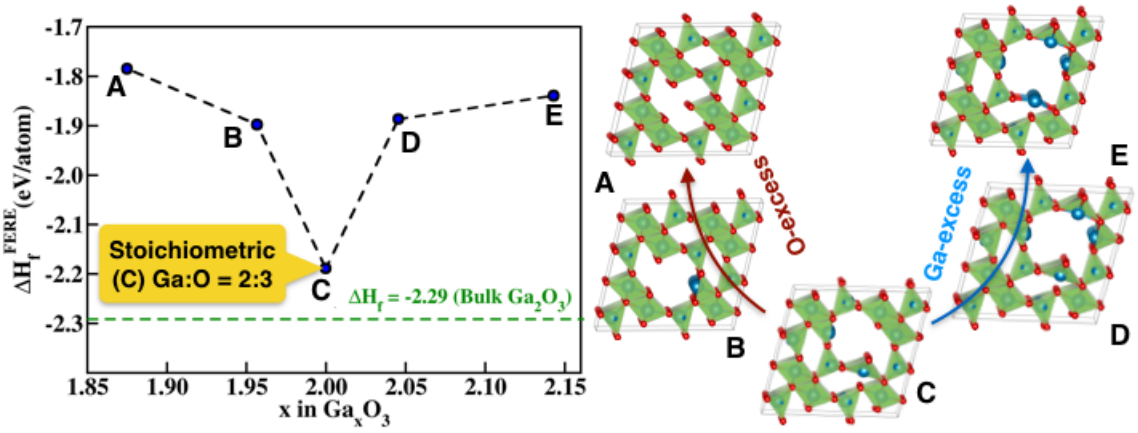

Fig. 3 Left panel: Defect formation energy (ΔH_f^{FERE}) with respect to deviation from stoichiometric vacancy concentration. Right panel: stoichiometric (C) and non-stoichiometric (A,B,D,E) defect structures with 1D Vacancy channel along y (V-2-type) has been shown.

by ~0.03 eV in energy with respect to the Γ point, thus does not substantially affect the magnitude of the band gap. In practice, the negligibly small energy difference between indirect and direct gaps and strong dipolar transition effectively make β-Ga_2O_3 a direct-gap material. This feature is consistent with the experimentally observed sharp absorption onset at ~4.9 eV.[52] In contrast to such wide band gap in pure β-Ga_2O_3, we find a huge reduction in the band gap (see Table 2) after formation of the extended vacancy channel. E_g of V-2 (2.63 eV) is 2.17 eV lesser than the E_g of pristine β-Ga_2O_3 (see Figure 5b). Hence, the sensitivity of V-2 in the visible region appears appealing for the photocatalysis and optoelectronics. It is evident that β-Ga_2O_3 retains its direct-gap nature for both the perfect-crystalline and porous-crystalline structures while the gap states always lie at the Γ point. However, V-2 exhibits a much flatter valence band (Figure 5b), indicating a larger hole effective mass and lower hole-mobility. The low energy conduction band dispersion curves avoid crossing with each other, which is different from the case of pristine β-Ga_2O_3. We also note that the porosity-induced defect in the system does not attribute to the localised mid-gap state. Instead, the whole va-

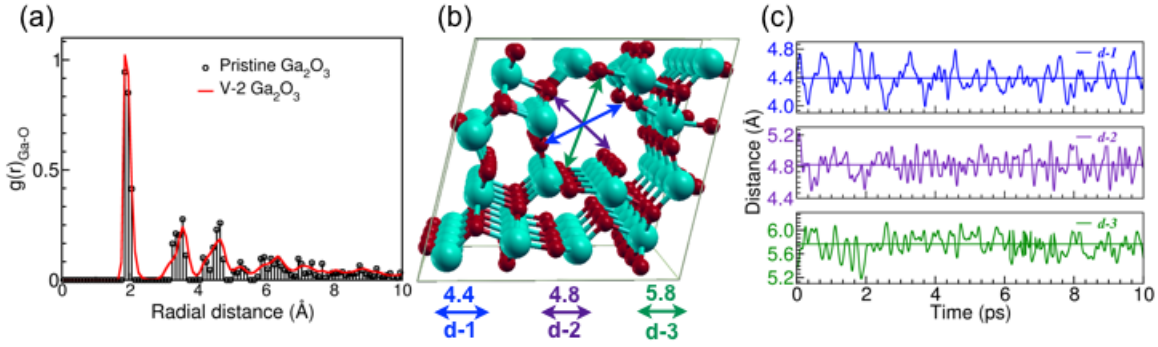

Fig. 4 (a) Radial pair distribution function, g(r), vs. r for pure β-Ga_2O_3 (black points and line) and V-2 (red line) are shown. (b) Pore diameter of V-2 (DFT-optimised structure), and (c) fluctuation in pore diameters as obtained from *ab initio* molecular dynamics simulations at T = 300 K (for 10 ps) and constant pressure (1 atm) are shown.

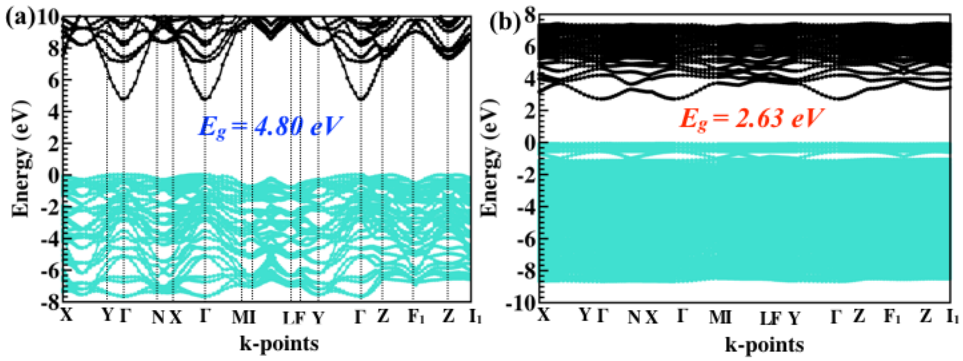

Fig. 5 HSE06 band structure of (a) pure β-Ga_2O_3 and (b) V-2 are shown along the defined path in the Brillouin zone. The high-symmetry points are schematically indicated in the Brillouin zone drawn in Figure 1 in ESI.

lence band is connected, without separate defect bands. Such characteristic feature appears due to the stoichiometric configuration of V-2. Nevertheless, the reduction of the band gap is significant. Since both Al_2O_3 and Ga_2O_3 have been used for catalysis, the absorption of the optical light can make Ga_2O_3 a potential optoelectronic catalytic material with a feature unavailable for Al_2O_3.

The site-resolved PDOS (see Figure 6a,b) indicates that atoms residing in the vicinity of the vacancy channel in V-2 contribute predominantly to the band extrema states. CBM is predominantly contributed by 4*s*/*p* states of the coordinatively unsaturated Ga and VBM is originated solely from the coordinatively unsaturated O-sites (see Figure 6b). In contrast, for pure β-Ga_2O_3, VBM has the dominant characteristics of the O-2*p* states and CBM originates from the mixed Ga-4*s*/O-2*s* states(see Figure 6a). Hence, site-resolved PDOS proves the spatial distinction between VBM and CBM, especially for V-2. Notably, VBM becomes more localised in V-2 compared to pure β-Ga_2O_3. On the other hand, the electron delocalises along the vacancy channel for the lowest CB (see upper right panel in Figure 7). Such delocalisation of charges in the CB is attributed to the diffused orbital of unsaturated Ga-sites which couple strongly along the channel direction. Understanding such vacancy-dependent electronic structures is important to tune the photocatalytic activity of the junction between the vacancy line and the bulk crystal. This is particularly useful to determine the active sites in the β-Ga_2O_3 based catalysts.

3.4 Optical properties

We have computed the optical absorption spectra of pure β-Ga_2O_3 (see Figure 8) which well corroborates with the experimental reports.[53] For pure β-Ga_2O_3, the absorption spectra typically exhibits a discreet cut off absorption edge which is also in line with the previous experimental measurements showing that transmittance spectra exhibit a steep absorption edge at 255-260 nm and almost full transparency to the NIR wavelength range for the samples with low electron concentration.[53] We have applied the same computational methodology for V-2 as that for the pure β-Ga_2O_3. V-2 exhibits a significant reduction of the refractive index compared to the pure β-Ga_2O_3. The more appealing finding is that the V-2 structure appears as a light absorber even at 1.47 eV lower in energy (see Figure 8), while the pure β-Ga_2O_3 is insensitive to visible light. Such finite absorption coefficient in the visible and infrared region for V-2 is important for versatile application of Ga_2O_3. Vacancy-induced modulation of optical absorption spectra can be understood by analysing the states involved in low-energy transitions (see Figure 9). Band-extrema state charge densities, the relative positions of the energy levels, and their contribution to the optical absorption spectrum are shown in Figure 9. We find that the optical absorption in porous-crystalline β-Ga_2O_3 (V-2) can be attributed to the intrinsic band-to-band transition i.e. from the valence band to the conduction band. The origin of the red shift of the absorption edge for V-2 is due to the band gap reduction. The initial absorption coeffi-

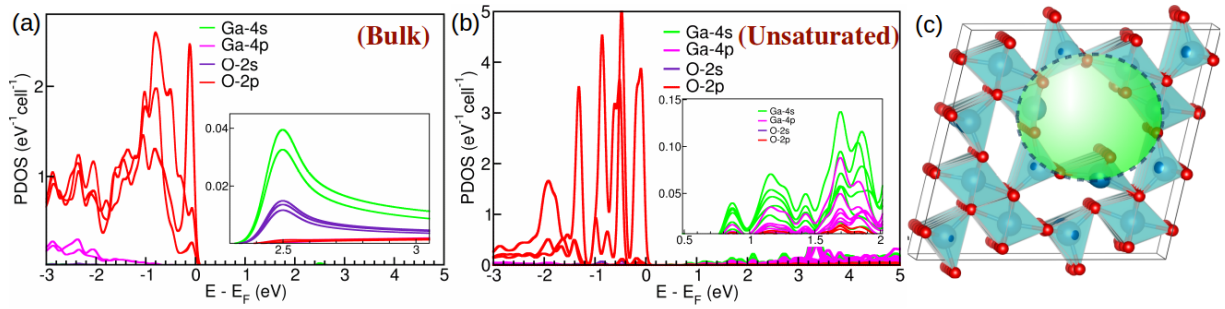

Fig. 6 (a) Site resolved PDOS (at gamma point; PBE/PAW level of theory) for bulk Ga/O sites are shown; (b) Orbital contributions from the unsaturated Ga/O sites in V-2 are plotted; In each cases (a and b), the low energy conduction states have been zoomed in the inset figures. (c) green-shaded region indicates the unsaturated Ga/O sites adjacent to the vacancy channel in V-2, as plotted in b subfigure.

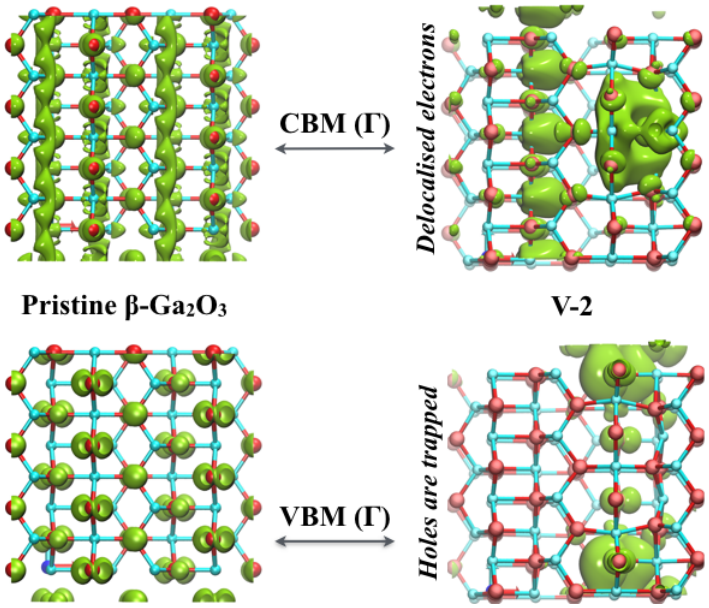

Fig. 7 The charge density distribution of the highest VB and lowest CB at the PBE/PAW level of theory for pristine (left panel) and porous-crystalline (V-2) β-Ga_2O_3 (right panel) are shown.

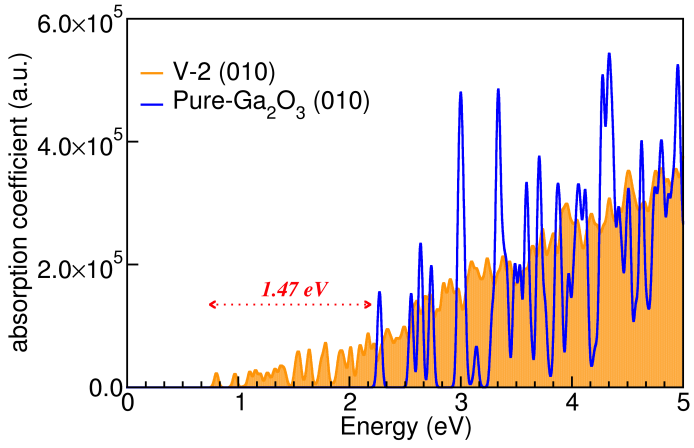

Fig. 8 Computed optical absorption spectra of pure β-Ga_2O_3 and porous-crystalline (V-2) β-Ga_2O_3 are shown. This calculation is done using PBE functional.

cient near the threshold is lesser for V-2, compared to the sharp increase in the perfect crystalline β-Ga_2O_3. This is due to the charge separation between the VBM and the CBM in the V-2 structure as shown in Figure 7. Such spatial separation of the electron and the hole reduces the oscillator strength of V-2 compared to the bulk β-Ga_2O_3. These behaviours are further confirmed by the charge density distribution of the highest VB and lowest CB, as shown in Figure 3 in ESI.

We note that for pure β-Ga_2O_3, VBM and CBM are not spatially separated because of the intersection region due to mixed Ga-O contribution in the CBM. In contrast, for V-2, CBM is solely contributed by the coordination-unsaturated Ga-sites and VBM is originated from the coordination-unsaturated O-sites, which leads to spatially distinct regions between the electron and the hole. Notably, the unsaturated O-atoms in the vicinity of the channel undergo a reduction of coordination number from three to two, in which O atoms resemble an sp^3 character with two lone pair of electron on O and the Ga-O-Ga angle becomes 112°. In contrast, for the bulk β-Ga_2O_3, the Ga-O-Ga angles consisting of 3-coordinated O are 95°, 102°, and 107°. The same for the 4-coordinated O are in the range of 94-114°. Hence, the 2-coordinated O-sites in the V-2 structure has a significantly different bonding motif which is not found in the bulk Ga_2O_3. This results in a more localized hole state. On the other hand, electrons can migrate across the unsaturated Ga-sites, thus should have a larger electron mobility.

Having said above, we emphasise on two key-points, i.e., the reduction of the band gap and the electron-hole separation when such nano-channel exists in β-Ga_2O_3. We also provide the design principle for such systems, but do not insist on the exact size of the channel. We believe similar band gap reduction can also happen for larger channel since the band edge states are located at some local surface-atom-bonding environment which also exists in the larger channel. To test this hypothesis, we have considered a model with larger pore-diameter, as shown in Figure 4 in ESI. Even for the larger pore-sized Ga_2O_3, we find the band gap (PBE-calculated) of 0.65 eV, which is comparable to the gap of ~0.70 eV as found in case of almost half-sized porous channel. Moreover, the electron and the hole states for the bigger channel (see Figure 5 in ESI) reside at spatially different locations, as found for the smaller channel too (see the right panel of Figure 7). So, the

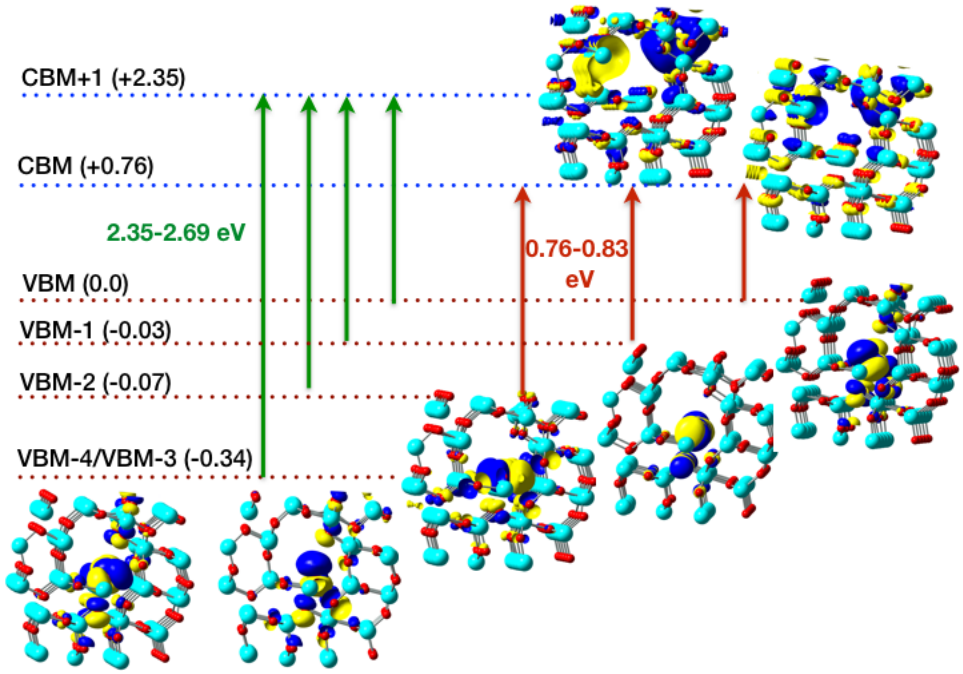

Fig. 9 Relative energies of the states involved in low-energy optical transitions in V-2 and the corresponding wavefunction plots in real space are shown.

basic features, i.e., the reduced band-gap and spatial separation of electron-hole states for porous-crystalline Ga_2O_3 is robust, and does not change significantly with the size of the pore. Hence, we can infer that the V-2 like porous-crystalline structure represents a model approach for efficient separation of electron and hole in an overall charge neutral system.

4 Conclusions

In summary, we find that the 1D vacancy channel in β-Ga_2O_3 (V-2) made up of Ga- and O- vacancy at stoichiometric ratio is thermodynamically and kinetically stable. The extended vacancy in porous-crystalline β-Ga_2O_3 confers the sensitivity in the visible regime (E_g = 2.63 eV) unlike the optically transparent pure β-Ga_2O_3 (E_g = 4.8 eV). Such Vis-sensitivity can be useful for the photoelectron applications like photocatalysis. The low-energy (at VIS-regime) optical transitions originate from the electronic states belonged to the vacancy-induced unsaturated atomic sites. The O-Ga-O coordination motif in the vicinity of the vacancy-channel results in a dipole-allowed transition in the visible regime. Compared to the bulk β-Ga_2O_3, porous-crystallinity leads to a weaker absorption onset. This is due to the electron-hole separation in the V-2 system. Coordination-unsaturated sp^3 O-sites act as pseudo electron-donor and Ga-sites act as pseudo electron-acceptor. As a result, the extended vacancy channel which is overall charge neutral, results in spatial separation of the electron and the hole. The low recombination rate between electron and hole should also be beneficial for photocatalytic application. Hence, we conjecture that β-Ga_2O_3 can prove itself as a versatile electronic material operating at both the UV and VIS regime after engineering the vacancy states. Moreover, our strategy of creating porous channel in the crystal framework to tune the bulk properties should motivate the experimentalists for such endeavours. We finally note that our vacancy-channel system can be used as a model system for porous Ga_2O_3. We expect many of the principles as found in this study can also be extended to other porous Ga_2O_3 structures.

We acknowledge the computational resources of the National Energy Research Scientific Computing Center. We thank the support by the National Natural Science Foundation of China (grand No. 11574304 and 11774338), Chinese Academy of Science-Peking University Pioneer Cooperation Team, and the Youth Innovation Promotion Association CAS (grand No. 2016109). LWW thanks the Director, Office of Science (SC), Basic Energy Science (BES), Materials Sciences and Engineering Division (MSED), of the US Department of Energy (DOE) under contract no. DE-AC02-05CH11231 through the Materials Theory program (KC2301).

References

1 M. Higashiwaki, K. Sasaki, A. Kuramata, T. Masui and S. Yamakoshi, *Applied Physics Letters*, 2012, **100**, 013504.
2 K. Sasaki, M. Higashiwaki, A. Kuramata, T. Masui and S. Yamakoshi, *Journal of Crystal Growth*, 2013, **378**, 591–595.
3 M. Calatayud, S. Collins, M. Baltanas and A. Bonivardi, *Physical Chemistry Chemical Physics*, 2009, **11**, 1397–1405.
4 H. Tsuneoka, K. Teramura, T. Shishido and T. Tanaka, *The Journal of Physical Chemistry C*, 2010, **114**, 8892–8898.
5 L. Yuliati, H. Itoh and H. Yoshida, *Chemical Physics Letters*, 2008, **452**, 178–182.
6 H.-a. Park, J. H. Choi, K. M. Choi, D. K. Lee and J. K. Kang, *Journal of Materials Chemistry*, 2012, **22**, 5304–5307.
7 K. Ulman, M.-T. Nguyen, N. Seriani, S. Piccinin and R. Gebauer, *ACS Catalysis*, 2017, **7**, 1793–1804.
8 Y. Inoue, *Energy & Environmental Science*, 2009, **2**, 364–386.
9 X. Chen, S. Shen, L. Guo, S. S. Mao *et al.*, *Chemical reviews*, 2010, **110**, 6503.
10 K. Maeda, K. Teramura, N. Saito, Y. Inoue, H. Kobayashi and K. Domen, *Pure and applied chemistry*, 2006, **78**, 2267–2276.
11 A. J. Rettie, W. D. Chemelewski, D. Emin and C. B. Mullins, *The journal of physical chemistry letters*, 2016, **7**, 471–479.
12 S. Lany and A. Zunger, *Physical Review B*, 2009, **80**, 085202.
13 C. Tagusagawa, A. Takagaki, A. Iguchi, K. Takanabe, J. N. Kondo, K. Ebitani, S. Hayashi, T. Tatsumi and K. Domen, *Angewandte Chemie*, 2010, **122**, 1146–1150.
14 N. Syed, A. Zavabeti, M. Mohiuddin, B. Zhang, Y. Wang, R. S. Datta, P. Atkin, B. J. Carey, C. Tan and J. van Embden, *Advanced Functional Materials*, 2017.
15 J. Cheng, Y. Wang, Y. Xing, M. Shahid and W. Pan, *Applied Catalysis B: Environmental*, 2017, **209**, 53–61.
16 M. Kruk, M. Jaroniec, C. H. Ko and R. Ryoo, *Chemistry of materials*, 2000, **12**, 1961–1968.
17 S.-Z. Chu, S. Inoue, K. Wada, D. Li, H. Haneda and S. Awatsu, *The Journal of Physical Chemistry B*, 2003, **107**, 6586–6589.
18 R. Asahi, T. Morikawa, T. Ohwaki, K. Aoki and Y. Taga, *science*, 2001, **293**, 269–271.
19 K. P. Loh, Q. Bao, G. Eda and M. Chhowalla, *Nature chemistry*, 2010, **2**, 1015–1024.
20 J. Low, J. Yu, M. Jaroniec, S. Wageh and A. A. Al-Ghamdi, *Advanced Materials*, 2017.
21 S. Geller, *The Journal of Chemical Physics*, 1960, **33**, 676–684.
22 M. Marezio and J. Remeika, *The Journal of Chemical Physics*, 1967, **46**, 1862–1865.
23 H. He, R. Orlando, M. A. Blanco, R. Pandey, E. Amzallag, I. Baraille and M. Rérat, *Physical Review B*, 2006, **74**, 195123.
24 J. Varley, J. Weber, A. Janotti and C. Van de Walle, *Applied Physics Letters*, 2010, **97**, 142106.
25 B. Cheng and E. T. Samulski, *Journal of Materials Chemistry*, 2001, **11**, 2901–2902.
26 S. Sharma and M. K. Sunkara, *Journal of the American Chemical Society*, 2002, **124**, 12288–12293.
27 H. Oveisi, C. Anand, A. Mano, S. S. Al-Deyab, P. Kalita, A. Beitollahi and A. Vinu, *Journal of Materials Chemistry*, 2010, **20**, 10120–10129.
28 L. Nagarajan, R. A. De Souza, D. Samuelis, I. Valov, A. Börger, J. Janek, K.-D. Becker, P. C. Schmidt and M. Martin, *Nature materials*, 2008, **7**, 391.
29 X. Zheng and L. Zhang, *Energy & Environmental Science*, 2016, **9**, 2511–2532.
30 M.-G. Ju, X. Wang, W. Liang, Y. Zhao and C. Li, *Journal of Materials Chemistry A*, 2014, **2**, 17005–17014.
31 G. Carja, E. F. Grosu, M. Mureseanu and D. Lutic, *Catalysis Science & Technology*, 2017.
32 F. Li, L. Zhang and R. M. Metzger, *Chemistry of materials*, 1998, **10**, 2470–2480.
33 J. Mei, Y. Shao, S. Lu, Y. Ma and L. Ren, *Journal of Materials Science*, 2018, **53**, 3375–3387.
34 J. Chmiola, G. Yushin, Y. Gogotsi, C. Portet, P. Simon and P.-L. Taberna, *Science*, 2006, **313**, 1760–1763.
35 P. Giannozzi, S. Baroni, N. Bonini, M. Calandra, R. Car, C. Cavazzoni, D. Ceresoli, G. L. Chiarotti, M. Cococcioni and I. Dabo, *Journal of Physics: Condensed Matter*, 2009, **21**, 395502.
36 J. P. Perdew, K. Burke and Y. Wang, *Physical Review B*, 1996, **54**, 16533.
37 B. Hammer, L. B. Hansen and J. K. Nørskov, *Physical Review B*, 1999, **59**, 7413.
38 J. Heyd, G. E. Scuseria and M. Ernzerhof, *The Journal of Chemical Physics*, 2003, **118**, 8207–8215.
39 J. Heyd, G. E. Scuseria and M. Ernzerhof, *The Journal of Chemical Physics*, 2006, **124**, 219906.
40 L.-W. Wang, *All the Programs Can Be Obtained from: http://www.pwmat.com*.
41 P. E. Blöchl, *Physical Review B*, 1994, **50**, 17953.
42 S. Grimme, J. Antony, S. Ehrlich and H. Krieg, *The Journal of Chemical Physics*, 2010, **132**, 154104.
43 T. Böker, R. Severin, A. Müller, C. Janowitz, R. Manzke, D. Voß, P. Krüger, A. Mazur and J. Pollmann, *Physical Review B*, 2001, **64**, 235305.
44 V. Stevanović, S. Lany, X. Zhang and A. Zunger, *Physical Review B*, 2012, **85**, 115104.
45 J. M. Soler, E. Artacho, J. D. Gale, A. García, J. Junquera, P. Ordejón and D. Sánchez-Portal, *Journal of Physics: Condensed Matter*, 2002, **14**, 2745.
46 P. Ordejón, E. Artacho and J. M. Soler, *Phys. Rev. B*, 1996, **53**, R10441–R10444.
47 D. Sánchez-Portal, P. Ordejon, E. Artacho and J. M. Soler, *International Journal of Quantum Chemistry*, 1997, **65**, 453–461.
48 S. Geller, *The Journal of Chemical Physics*, 1960, **33**, 676–684.
49 R. Roy, V. Hill and E. Osborn, *Journal of the American Chemical Society*, 1952, **74**, 719–722.
50 C. Janowitz, V. Scherer, M. Mohamed, A. Krapf, H. Dwelk, R. Manzke, Z. Galazka, R. Uecker, K. Irmscher and R. Fornari, *New Journal of Physics*, 2011, **13**, 085014.
51 S. Stepanov, V. Nikolaev, V. Bougrov and A. Romanov, *Rev. Adv. Mater. Sci*, 2016, **44**, 63–86.
52 C. Janowitz, V. Scherer, M. Mohamed, A. Krapf, H. Dwelk, R. Manzke, Z. Galazka, R. Uecker, K. Irmscher, R. Fornari, M. Michling, D. SchmeiSSer, J. R Weber, J. B. Varley and C. G. Van de Walle, *New Journal of Physics*, 2011, **13**, 085014.
53 I. Bhaumik, R. Bhatt, S. Ganesamoorthy, A. Saxena, A. Karnal, P. Gupta, A. Sinha and S. Deb, *Applied optics*, 2011, **50**, 6006–6010.